HHS Public Access

Author manuscript

Biomed Phys Eng Express. Author manuscript; available in PMC 2023 October 18.

Published in final edited form as:

Biomed Phys Eng Express. ; 8(6): . doi:10.1088/2057-1976/ac9848.

Feasibility of 4D VMAT-CT

Xiaodong Zhao[1], **Rui Zhang**[2,3,*]

[1]Department of Radiation Oncology, Washington University in St. Louis, St. Louis, MO, USA

[2]Department of Physics and Astronomy, Louisiana State University, Baton Rouge, LA, USA

[3]Department of Radiation Oncology, Mary Bird Perkins Cancer Center, Baton Rouge, LA, USA

Abstract

Objective.—Feasibility of three-dimensional (3D) tracking of volumetric modulated arc therapy (VMAT) based on VMAT–computed tomography (VMAT-CT) has been shown previously by our group. However, 3D VMAT-CT is not suitable for treatments that involve significant target movement due to patient breathing. The goal of this study was to reconstruct four-dimensional (4D) VMAT-CT and evaluate the feasibility of tracking based on 4D VMAT-CT.

Approach.—Synchronized EPID images of phantoms and linac log were both sorted into four phases, and VMAT-CT+ was generated in each phase by fusing reconstructed VMAT-CT and planning CT using rigid or deformable registration. Dose was calculated in each phase and was registered to the mean position planning CT for 4D dose reconstruction. Trackings based on 4D VMAT-CT+ and 4D cone beam CT (CBCT) were compared. Potential uncertainties were also evaluated.

Main results.—Tracking based on 4D VMAT-CT+ was accurate, could detect phantom deformation and/or change of breathing pattern, and was superior to that based on 4D CBCT. The impact of uncertainties on tracking was minimal.

Significance.—Our study shows it is feasible to accurately track position and dose based on 4D VMAT-CT for patients whose VMAT treatments are subject to respiratory motion. It will significantly increase the confidence of VMAT and is a clinically viable solution to daily patient positioning, in vivo dosimetry and treatment monitoring.

Keywords

Volumetric modulated arc therapy; computed tomography; four-dimensional; respiratory motion; lung cancer; upper abdomen cancer

[*]Corresponding author: Rui Zhang, Department of Physics and Astronomy, Louisiana State University, Baton Rouge, LA, USA. Phone: 225-215-1132; rzhang@lsu.edu.

Conflict of interest statement

The authors have no conflicts of interest.

1. Introduction

Respiratory motion is a major obstacle to radiotherapy for patients with lung or upper abdomen cancer and causes both geometric and dosimetric uncertainties. Current radiotherapy planning for those patients usually requires a generous margin around the tumor to account for possible uncertainties, which will limit the total dose that can be safely delivered. To consider respiratory motion, a four-dimensional (4D) computed tomography (CT) is usually obtained before treatment for planning purpose (Low et al., 2003). Currently most linear accelerators (linacs) do not have 4D kilovoltage (kV) cone beam CT (CBCT) option during treatment (Takahashi et al., 2013). Instead, a three-dimensional (3D) or 4D CBCT before each treatment fraction is acquired. In many clinics, CBCT is performed before and after lung stereotactic body radiotherapy (SBRT) to help with patient setup and determine the patient's final position for dose estimation (Purdie et al., 2007; Yin et al., 2008; Sonke et al., 2009; Lambrecht et al., 2016). These imaging techniques do not track tumor location during beam delivery, while it is well known that the movement of thoracic and abdominal organs and tumors can vary unpredictably minute by minute (Seppenwoolde et al., 2002; Dhont et al., 2018). They also introduce extra imaging dose, e.g., CBCT can introduce 1~29 cGy in each fraction to healthy tissues depending on patient size and scan site (Murphy et al., 2007; Ding and Coffey, 2009), and 4D CT or CBCT will introduce even higher dose to the patients (Murphy et al., 2007; Cooper et al., 2019). In addition, each CT scan will introduce several hundred to several thousand dollars charge (Zhou et al., 2018), which is a significant burden to the patients, especially when imaging is performed frequently.

Among radiotherapy modalities, VMAT has been increasingly used and shows specific advantages for various cancer sites because of its short treatment time and improved dose conformity (Verbakel et al., 2009; Ong et al., 2010; Popescu et al., 2010; Qiu et al., 2010; Quan et al., 2012; Teoh et al., 2013; Nichols et al., 2014; Jin et al., 2019). 3D megavoltage (MV) CT reconstruction using portal images acquired during VMAT, so called "VMAT-CT", was first proposed in 2010 (Poludniowski et al., 2010). Our group previously demonstrated the feasibility of 3D tracking and adaptation of VMAT based on VMAT-CT (Zhao and Zhang, 2020). However, 3D VMAT-CT is not sufficient for treatments that involve significant target movement due to patient breathing. Kida et al. (2011) developed a 4D version of VMAT-CT and compared two tracking methods that were based on 4D VMAT-CT and in-treatment kV CBCT for two patients. They applied a constraint on multi-leaf collimator (MLC) motion to ensure target was always exposed during treatment, which is not clinically realistic. There are some other shortcomings of 4D VMAT-CT like limited field of view (FOV), low image quality and no electron density information.

The goal of this study is to extend our previous study and develop a technique to track lung VMAT based on 4D VMAT-CT. Comparison with tracking based on 4D CBCT and uncertainties associated with 4D VMAT-CT were also evaluated. As the previous studies (Kida et al., 2011; Zhao and Zhang, 2020; de Bruin et al., 2021), tracking in this study refers to the tracing of intrafraction patient position, respiratory pattern and dose, rather than the adaptation of MLC aperture to the tumor position in real time during treatment.

2. Materials and methods

2.1. Phantoms, treatment planning, and data collection

A QUASAR™ programmable respiratory motion phantom (Modus Medical Devices Inc., London, Ontario, Canada) was used in this study (figure 1(a)). The phantom has an acrylic body and a motor driving a cedar wood cylinder mimicking movement of the lung. The cedar wood cylinder splits in the middle and has a 3-cm diameter ball mimicking a tumor. We set up the QUASAR phantom to have 2 breathing patterns: one regular sine wave with a period of 4 second and amplitude of 10 mm; four irregular breathing patterns extracted from a real patient's breathing signal, with the period ranging between 3 and 5 second, and the amplitude ranging between 1 and 2 cm. An in-house deformable lung phantom (Zhao and Zhang, 2020) was also used in this study (figure 1(b)). The deformable tumor which is a small balloon filled with gel was tied with strings on both ends: one end of it was fixed and the other end was attached to the QUASAR phantom to drive the tumor with desired breathing pattern and to deform the tumor.

4D cine planning CT of the QUASAR phantom and the deformable phantom were acquired with a 16-slice GE LightSpeed CT scanner (GE Medical Systems, Milwaukee, WI, USA) and reconstructed with Advantage 4D (GE Healthcare, Waukesha, WI, USA). While acquiring 4D planning CT, a respiratory signal was acquired by the Real-Time Position Management (RPM) Respiratory Gating system (Varian Medical Systems, Palo Alto, CA, USA) concurrently, and a probability density function (PDF) of tumor position versus time was obtained. The gross tumor volume (GTV) was delineated on all 4 phases (max exhale, mid-exhale-inhale, max inhale, and mid-inhale-exhale) of 4D planning CT by setting a HU (Hounsfield unit) threshold. Mean position of the PDF was calculated, and from the four-phase planning CT data sets, one phase's data set was chosen as the mean position planning CT (MPPCT) if that phase's GTV was closest to the mean position (Harsolia et al., 2008).

4D union plan was created for both QUASAR phantom and the deformable phantom in Pinnacle v9.10 treatment planning system (TPS) (Philips Medical Systems, Fitchburg, WI, USA). 4D union plans required the contour of the maximum intensity projection (MIP) of the target as internal target volume (ITV), which encompassed all possible locations of the tumor. Because phantoms do not have microscopic disease, we did not add an additional margin to account for that and expanded the ITV by 0.5 cm for setup error to construct the planning target volume (PTV). The 4D union plan accounts for respiratory motion measured during planning but does not account for changes in respiratory pattern throughout treatment, and is the standard practice for lung cancer radiotherapy in our clinic and many other clinics. VMAT Plans had two full 6 MV arcs, 45° (clockwise arc) or 135° (counterclockwise arc) collimator angle, 50 Gy heterogeneous prescription, 3×3×3 mm^3 dose grid, 1800~2000 total Monitor Units per fraction for 5 fractions. All plans were delivered by Elekta Versa linac (Elekta Oncology Systems, Crawley, UK).

2.2. Respiratory signal extraction and 4D VMAT-CT reconstruction

Normalized cross correlation (NCC) method (Kida et al., 2011) was used in this study to extract respiratory signals from EPID images acquired during VMAT. Without any external surrogates for tumor motion, shift of tumor between two consecutive EPID images was quantified by computing the NCC matrices of the same fixed area in the two EPID images. Repeating the process for all acquired images and matching the timestamp of EPID images stored in the iView system, a temporal tumor shift signal was acquired. However, this signal may contain pseudo components brought by gantry rotation that needed to be removed by applying a band pass filter, and 0.2 Hz and 1 Hz were used as thresholds in this study because patient breathing period is usually between 1 and 5 seconds (Kida et al., 2011). Unlike the plans in Kida *et al.* (Kida et al., 2011), target exposure was not guaranteed during the entire treatment because we did not set any constraint on MLC motion, which is the case for the clinical plans. To split the images into 4 phases, a time-based sorting method was used to get approximately same number of images in each phase in order to ensure image quality was comparable in each phase. VMAT-CT reconstruction was then carried out in each phase using the method reported by our group previously (Zhao and Zhang, 2020).

For the QUASAR phantom, rigid registration was performed between 4D VMAT-CT and MPPCT because we need to register reconstructed VMAT-CT in each phase to images with a clearly delineated contour of GTV and to generate a composite dose. After one phase's VMAT-CT was rigidly registered to MPPCT, the rigid registration matrix was applied to the moving cylinder insert in MPPCT and pixel-to-pixel electron density propagation was performed between registered region of MPPCT and VMAT-CT to create VMAT-CT+ in each phase. VMAT-CT+ includes patient position information during the treatment and has the same FOV and Hounsfield Unit (HU) scale as planning CT.

For the deformable phantom, deformable registration workflow in MIM (MIM Software Inc., Cleveland, OH) was used. First, a rigid alignment between each phase of VMAT-CT (primary dataset) and the MPPCT (secondary dataset) was performed, and the rigid transformation matrix was applied to the MPPCT. A local deformation was then performed, and local deformable matrix was applied to the local PTV area on the MPPCT to generate VMAT-CT+ in each phase.

2.3. Tracking based on 4D VMAT-CT

Figure 2 shows the workflow of 4D dose reconstruction in this study. Linac log and EPID images were individually timestamped and were synchronized by matching the MLC positions. The phase-dividing timestamps in EPID images were applied to the linac log to sort the MLC control points into four phases. Interpolation between control points was performed if any EPID timestamp fell between two control points' timestamps in linac log (Poulsen et al., 2012). Four new beam delivery files that were generated based on four phases' control points together with four sets of VMAT-CT+ DICOM images were imported into TPS. Dose was calculated in each phase on its corresponding VMAT-CT+, and each phases' dose matrix was registered using the transformation matrix derived from its VMAT-CT+'s registration to MPPCT.

For lung patients, certain clinics take 4D CBCT before each fraction for dose calculation (Sonke and Belderbos, 2010), and we therefore evaluated the dose differences based on 4D CBCT and 4D VMAT-CT+. For the QUASAR phantom, 4D planning CT captured the original breathing pattern (breathing 0), 4D CBCT was taken with a different breathing pattern (breathing 1) to mimic a possible change after planning CT, and 4D $CBCT_{ground}$ was taken after we changed the breathing pattern again to mimic a further change after CBCT and this pattern was used during VMAT (breathing 2). For the deformable phantom, 4D planning CT captured the original phantom geometry and breathing pattern (status 0), 4D CBCT was taken with a different breathing pattern and a different deformation of the phantom (status 1), and 4D $CBCT_{ground}$ was taken after we changed the breathing pattern and phantom deformation again and this status was used during VMAT (status 2). We extracted the respiratory signal from 4D CBCT projection images and reconstruct the composite dose the same way as we processed VMAT-CT images. 4D $CBCT_{ground}$ was used as the ground truth for both phantoms.

2.4. Uncertainty analysis

The main uncertainties that may affect the final dose in our study are from rigid or deformable registration. To evaluate the uncertainties brought by rigid registrations in 4D cases, we compared the reconstruction matrix between each phase of 4D VMAT-CT+ and MPPCT with that between each phase of 4D $CBCT_{ground}$+ (MPPCT registered to $CBCT_{ground}$) and MPPCT under the same breathing pattern for the QUASAR phantom. The impact of uncertainty from rigid registrations on dose was tested by shifting MPPCT the average uncertainty in each of X, Y, and Z-direction in a copy of the original plan to find out the dose difference. 3D gamma (Wendling et al., 2007) was also calculated with an acceptance criteria of 3% and 3mm.

To evaluate the uncertainty brought by deformable registrations in 4D cases, after registering MPPCT with each phase of 4D VMAT-CT+ and 4D $CBCT_{ground}$+ of the deformable phantom, we transferred PTV in MPPCT to each phase of 4D VMAT-CT+ and 4D $CBCT_{ground}$+ through deformable registration, and compared deformed PTV in VMAT-CT+ with that in $CBCT_{ground}$+. Hausdorff distance (HD), Mean distance to agreement (MDA), Dice similarity coefficient (DSC) and Jacobian determinant (Brock et al., 2017; Woerner et al., 2017) were evaluated. The impact of uncertainty from deformable registration on dose was tested by expanding or shrinking the PTV contour in each phase of 4D VMAT-CT+ by mean HD, calculating the dose in each phase, and registering back to MPPCT to get a new composite dose. 3D Gamma was also calculated.

3. Results

We verified both regular and irregular respiratory signals extracted from EPID images by comparing them with the input signals fed to the QUASAR phantom (figure 3). For regular breathing pattern, the setup period was 4 seconds and measured period was 3.99 seconds; for irregular breathing pattern, the mean setup period was 2.66 seconds and measured mean period was 2.68 seconds. Note the synchronization is for period, not amplitude, and the reason is we sorted EPID images into 4 phases based one time. Once the images were sorted

correctly, the reconstruction was only dependent on the selected images in that phase and did not reply on the amplitude of the respiratory signal.

Figure 4 shows the reconstructed 4 phases VMAT-CT images of both the QUASAR phantom and the deformable phantom. Locations of center of mass in phases 1 and 3 in VMAT-CT images of the QUASAR phantom were compared with 4D planning CT. For regular breathing pattern, planning CT showed 20 mm displacement while VMAT-CT showed 21 mm; for irregular breathing pattern, both planning CT and VMAT-CT showed 16 mm displacement.

Figure 5 shows dose calculation and tracking for the QUASAR phantom and 4D deformable phantom. Compared with the ground truth, VMAT-CT can accurately track the change of respiratory pattern and deformation (Gamma passing rate is always 100%), while pre-treatment CBCT cannot detect the changes during VMAT (Gamma passing rate is 85.5% and 81.3% for the QUASAR phantom and deformable phantom, respectively).

Tables 1 and 2 show rigid and deformable registration uncertainties, and each try is the averaged result from 4 phases. For the rigid registration, shifting the MPPCT the mean uncertainty in each direction induces the largest point dose uncertainty as 2.76, 0.59 and 2.81Gy in X, Y and Z-direction, respectively, and the 3D gamma passing rate is always 100%. For the deformable registration, the expansion or shrinkage of the mean HD reduces or increases the mean PTV dose by 0.97 Gy and 0.80 Gy, respectively, and the 3D gamma passing rate is 99.7%.

4. Discussion

We demonstrated the feasibility of 4D VMAT-CT reconstruction, geometry and dose tracking of lung VMAT based on 4D VMAT-CT. Kida et al. (2011) showed it is possible to extract respiratory signal from EPID images and reconstruct 4D VMAT-CT with target constantly exposed to radiation, while real clinic VMAT plans will not guarantee target is always exposed during treatment. In this study, we solved the main challenge that comes from the image quality of realistic MV projections with the target partially blocked by MLC, and we proved it's still possible to extract the respiratory trace and reconstruct VMAT-CT. The other novelty of this work is that there is no previous study about VMAT-CT-based 4D dose reconstruction or tracking, while we registered 4D VMAT-CT with MPPCT to create 4D VMAT-CT+ so that we can have the full FOV and the electron density information for dose calculation, and demonstrated the feasibility of dose accumulation workflow with 4D VMAT-CT.

The feasibility study presented here mainly focused on lung cancer. As long as there is enough density difference around the target region, the 4D VMAT-CT workflow could be applied to other sites with respiratory motion as well. At a minimum, we expect it is applicable to various types of thoracic cancers including lung cancers, thymic cancer, pleural cancer and tracheal cancer, esophageal cancer, upper abdomen cancer close to air cavities or bones, and cancer patients with fiducials.

Reconstruction of 4D VMAT-CT would eliminate extra imaging dose and treatment cost since the images come directly from the treatment beams and no extra hardware or diagnostic/therapeutic beam time is required, and can potentially reveal daily nonrigid anatomic changes, random positional errors, motion pattern change etc. during VMAT. None of the current imaging techniques can provide 3D or 4D patient's anatomy and dose information during RT. The emerging in-treatment kV CBCT (Kida et al., 2012), which is not available in most clinics, cannot achieve those without introducing substantial extra dose and/or treatment delay, suffers from the possible isocenter displacement between kV and MV treatment beams, and increased treatment cost. The emerging magnetic resonance imaging guided linear accelerator (MRI-linac) has very low availability and shortcomings such as not being able to image patients with metal-implants, image distortion, electron returning effect, long scan time and treatment duration, higher treatment cost and substantial structural investment. In contrast, our tool is a convenient, low-cost, harmless, effective imaging tool that can provide critical patient information

We determined NCC and time-based sorting are not sources of uncertainties. We verify the respiratory signal extracted from EPID images using NCC method side by side with the EPID images (the movement of target is visible on EPID images) to make sure the detected shift direction is correct. If certain image (at most a few) is sorted into the wrong phase using time-based sorting, which will be more likely in middle phases because target moves faster in those phases and sorting is slightly more error-prone, it will not make a big difference because the number of wrong images is a very small fraction of the total number of images, and the images in middle phases are usually already a little blurrier since the target moves faster. We verified the NCC method and time-based sorting using 8 patient beams and the results are all accurate compared to the ground truth.

Previous studies reported amplitude-based sorting shows superior results than time-based sorting (Lu et al., 2006; Wink et al., 2006; Kavanagh et al., 2009). However, there are usually 200 EPID images for a full arc lung SBRT beam, and each phase only has 50 images using time-based sorting. If amplitude-based sorting is used, there could be a big difference in the number of images in each phase: there would be more images in end-inhale or end-exhale phase when tumor slows down, and middle-phase VMAT-CT will then have poorer image quality than VMAT-CT in the end-exhale/inhale phases. In addition, NCC method may not always detect amplitude correctly because sometimes blurred images or blockage from the MLC would generate a wrong amplitude of target movement, so amplitude-based sorting could introduce more uncertainties. If the sampling rate of EPID image could be increased in the future, we can have less blurred image and amplitude-based sorting can be a possibility then.

As Kida et al. (2011), we adopted 4 phases in this 4D study, and VMAT-CT in each phase shows the average tumor position in that phase. Since we synchronized the image and the log file, the control points would also be correlated to the averaged position in that phase. With more phases, more accurate mapping of control points to target position could potentially be realized. The uncertainty brought by the limitation of four-phase binning still needs further investigation. Because the number of images in each phase is less after the total number is divided by four, improvement in image quality or sampling rate in 4D cases

is therefore even more important than in 3D cases as we discussed in our previous study (Zhao and Zhang, 2020). Better image quality will improve the accuracy of target tracking, and more images would allow us to divide the images into more phases and have better 4D dose evaluations.

VMAT-CT is currently reconstructed after treatment due to the limitation of computation speed. It does not replace 4D CBCT or kV cine images for patient setup purpose prior to beam delivery. Rather, it provides in-treatment tracking signal and dose accumulation after beam delivery. It essentially removes the necessity of pre-treatment imaging for adaptive therapy or dose tracking purpose, and can replace in-treatment and post-treatment CBCT because the patient's information during VMAT is already recorded. Current practice with external device for intrafraction motion management struggles to establish the target position relative to margin set before treatment or to establish the target position relative to organs at risk, because the external surrogate has insufficient correlations with internal motions (Fayad et al., 2011) and cannot provide anatomy information. The additional in-treatment imaging may solve the problem, but will introduce extra dose and treatment cost. With VMAT-CT, if there is positional inconsistency, 4D dose reconstruction can help to evaluate where the hot and cold spots are and initiate the offline adaptive re-planning.

Deformable image registration has been discussed extensively in the literature. Lung deformable registration uncertainty presented in this study is consistent with the previous studies (Kashani et al., 2008; Ostergaard Noe et al., 2008; Brock, 2010; Niu et al., 2012). Similar to Niu et al. (2012), we found the resulting dose uncertainty is largest in steep dose gradient region. For further clinical applications, comprehensive commissioning and quality assurance are required according to AAPM Task Group 132 (Brock et al., 2017). The MIDRAS study (Brock, 2010) showed the deformable registration uncertainty increases due to the lack of anatomical markers and contrast in certain anatomical region such as liver, which is a similar challenge that VMAT-CT faces. Our group is actively developing novel methods to preprocess EPID images, remove the blurred region, improve the image quality of EPID images and subsequent VMAT-CT, which would reduce deformable registration uncertainty and increase confidence in dose accumulation. There is a strong need for commercially available deformable phantom which would also help with establishing a robust clinical dose accumulation workflow.

One potential error that needs further investigation is the possible discrepancy between delivered beams and recorded linac log. Several studies (Wijesooriya et al., 2012; Chuang et al., 2020) have reported the discrepancy between the actual machine parameters at treatment and information recorded in log files. Since we relied on the machine parameters in log files and interpolated control points for dose reconstruction in this study, there could be an additional source of error that needs more assessment. The EPID images reveal some machine parameters such as MLC positions, and a careful calibration is needed to extract this information from EPID to synchronize with and interpolate the control points in log files.

In conclusion, we extended our previous 3D study to 4D scenarios, reconstructed 4D VMAT-CT using realistic patient breathing patterns, calculated 4D doses and validated them.

4D VMAT-CT can be a very useful tool for respiratory signal tracking and dose verification for cancer patients whose treatments are subject to the motion issue.

Acknowledgements

This work was supported by National Institutes of Health (grant no. K22CA204464), American Cancer Society (grant no. RSG-22-030-01-CTPS), Louisiana Board of Regents Proof-of-Concept/Prototyping Initiative Fund, Louisiana State University LIFT^2 Fund, and Louisiana State University Faculty Research Grant.

References

Brock KK 2010 Results of a multi-institution deformable registration accuracy study (MIDRAS) Int J Radiat Oncol Biol Phys 76 583–96 [PubMed: 19910137]

Brock KK, Mutic S, McNutt TR, Li H and Kessler ML 2017 Use of image registration and fusion algorithms and techniques in radiotherapy: Report of the AAPM Radiation Therapy Committee Task Group No. 132 Med Phys 44 e43–e76 [PubMed: 28376237]

Chuang KC, Giles W and Adamson J 2020 On the use of trajectory log files for machine & patient specific QA Biomedical physics & engineering express 7

Cooper BJ, O'Brien RT, Shieh CC and Keall PJ 2019 Real-time respiratory triggered four dimensional cone-beam CT halves imaging dose compared to conventional 4D CBCT Phys Med Biol 64 07NT1

de Bruin K, Dahele M, Mostafavi H, Slotman BJ and Verbakel W 2021 Markerless Real-Time 3-Dimensional kV Tracking of Lung Tumors During Free Breathing Stereotactic Radiation Therapy Advances in radiation oncology 6 100705 [PubMed: 34113742]

Dhont J, Vandemeulebroucke J, Burghelea M, Poels K, Depuydt T, Van den Begin R, Jaudet C, Collen C, Engels B, Reynders T, Boussaer M, Gevaert T, De Ridder M and Verellen D 2018 The long- and short-term variability of breathing induced tumor motion in lung and liver over the course of a radiotherapy treatment Radiotherapy and Oncology 126 339–46 [PubMed: 28992962]

Ding GX and Coffey CW 2009 Radiation Dose from Kilovoltage Cone Beam Computed Tomography in an Image-Guided Radiotherapy Procedure International Journal of Radiation Oncology Biology Physics 73 610–7 [PubMed: 19147025]

Fayad H, Pan T, Clement JF and Visvikis D 2011 Technical Note: Correlation of respiratory motion between external patient surface and internal anatomical landmarks Medical Physics 38 3157–64 [PubMed: 21815390]

Harsolia A, Hugo GD, Kestin LL, Grills IS and Yan D 2008 Dosimetric advantages of four-dimensional adaptive image-guided radiotherapy for lung tumors using online cone-beam computed tomography Int J Radiat Oncol Biol Phys 70 582–9 [PubMed: 18207034]

Jin X, Lin B, Chen D, Li L, Han C, Zhou Y, Zheng X, Gong C, Chen M and Xie C 2019 Safety and outcomes of volumetric modulated arc therapy in the treatment of patients with inoperable lung cancer Journal of Cancer 10 2868–73 [PubMed: 31281463]

Kashani R, Hub M, Balter JM, Kessler ML, Dong L, Zhang L, Xing L, Xie Y, Hawkes D, Schnabel JA, McClelland J, Joshi S, Chen Q and Lu W 2008 Objective assessment of deformable image registration in radiotherapy: a multi-institution study Med Phys 35 5944–53 [PubMed: 19175149]

Kavanagh A, Evans PM, Hansen VN and Webb S 2009 Obtaining breathing patterns from any sequential thoracic x-ray image set Phys Med Biol 54 4879–88 [PubMed: 19636080]

Kida S, Masutani Y, Yamashita H, Imae T, Matsuura T, Saotome N, Ohtomo K, Nakagawa K and Haga A 2012 In-treatment 4D cone-beam CT with image-based respiratory phase recognition Radiological physics and technology 5 138–47 [PubMed: 22367851]

Kida S, Saotome N, Masutani Y, Yamashita H, Ohtomo K, Nakagawa K, Sakumi A and Haga A 2011 4D-CBCT reconstruction using MV portal imaging during volumetric modulated arc therapy Radiother Oncol 100 380–5 [PubMed: 21963287]

Lambrecht M, Melidis C, Sonke JJ, Adebahr S, Boellaard R, Verheij M, Guckenberger M, Nestle U and Hurkmans C 2016 Lungtech, a phase II EORTC trial of SBRT for centrally located lung tumours - a clinical physics perspective Radiat Oncol 11 7 [PubMed: 26791788]

Low DA, Nystrom M, Kalinin E, Parikh P, Dempsey JF, Bradley JD, Mutic S, Wahab SH, Islam T, Christensen G, Politte DG and Whiting BR 2003 A method for the reconstruction of four-dimensional synchronized CT scans acquired during free breathing Med Phys 30 1254–63 [PubMed: 12852551]

Lu W, Parikh PJ, Hubenschmidt JP, Bradley JD and Low DA 2006 A comparison between amplitude sorting and phase-angle sorting using external respiratory measurement for 4D CT Med Phys 33 2964–74 [PubMed: 16964875]

Murphy MJ, Balter J, Balter S, BenComo JA Jr., Das IJ, Jiang SB, Ma CM, Olivera GH, Rodebaugh RF, Ruchala KJ, Shirato H and Yin FF 2007 The management of imaging dose during image-guided radiotherapy: report of the AAPM Task Group 75 Med Phys 34 4041–63 [PubMed: 17985650]

Nichols GP, Fontenot JD, Gibbons JP and Sanders ME 2014 Evaluation of volumetric modulated arc therapy for postmastectomy treatment Radiat Oncol 9 66 [PubMed: 24571913]

Niu CJ, Foltz WD, Velec M, Moseley JL, Al-Mayah A and Brock KK 2012 A novel technique to enable experimental validation of deformable dose accumulation Med Phys 39 765–76 [PubMed: 22320786]

Ong CL, Verbakel WF, Cuijpers JP, Slotman BJ, Lagerwaard FJ and Senan S 2010 Stereotactic radiotherapy for peripheral lung tumors: a comparison of volumetric modulated arc therapy with 3 other delivery techniques Radiother Oncol 97 437–42 [PubMed: 21074878]

Ostergaard Noe K, De Senneville BD, Elstrom UV, Tanderup K and Sorensen TS 2008 Acceleration and validation of optical flow based deformable registration for image-guided radiotherapy Acta Oncol 47 1286–93 [PubMed: 18661435]

Poludniowski G, Thomas MD, Evans PM and Webb S 2010 CT reconstruction from portal images acquired during volumetric-modulated arc therapy Phys Med Biol 55 5635–51 [PubMed: 20826901]

Popescu CC, Olivotto IA, Beckham WA, Ansbacher W, Zavgorodni S, Shaffer R, Wai ES and Otto K 2010 Volumetric modulated arc therapy improves dosimetry and reduces treatment time compared to conventional intensity-modulated radiotherapy for locoregional radiotherapy of left-sided breast cancer and internal mammary nodes Int J Radiat Oncol Biol Phys 76 287–95 [PubMed: 19775832]

Poulsen PR, Schmidt ML, Keall P, Worm ES, Fledelius W and Hoffmann L 2012 A method of dose reconstruction for moving targets compatible with dynamic treatments. pp 6237–46

Purdie TG, Bissonnette JP, Franks K, Bezjak A, Payne D, Sie F, Sharpe MB and Jaffray DA 2007 Cone-beam computed tomography for on-line image guidance of lung stereotactic radiotherapy: localization, verification, and intrafraction tumor position Int J Radiat Oncol Biol Phys 68 243–52 [PubMed: 17331671]

Qiu JJ, Chang Z, Wu QJ, Yoo S, Horton J and Yin FF 2010 Impact of volumetric modulated arc therapy technique on treatment with partial breast irradiation Int J Radiat Oncol Biol Phys 78 288–96 [PubMed: 20444558]

Quan EZM, Li XQ, Li YP, Wang XC, Kudchadker RJ, Johnson JL, Kuban DA, Lee AK and Zhang XD 2012 A Comprehensive Comparison of IMRT and VMAT Plan Quality for Prostate Cancer Treatment International Journal of Radiation Oncology Biology Physics 83 1169–78 [PubMed: 22704703]

Seppenwoolde Y, Shirato H, Kitamura K, Shimizu S, van Herk M, Lebesque JV and Miyasaka K 2002 Precise and real-time measurement of 3D tumor motion in lung due to breathing and heartbeat, measured during radiotherapy International Journal of Radiation Oncology Biology Physics 53 822–34 [PubMed: 12095547]

Sonke J-J and Belderbos J 2010 Adaptive radiotherapy for lung cancer Seminars In Radiation Oncology 20 94–106 [PubMed: 20219547]

Sonke JJ, Rossi M, Wolthaus J, van Herk M, Damen E and Belderbos J 2009 Frameless stereotactic body radiotherapy for lung cancer using four-dimensional cone beam CT guidance Int J Radiat Oncol Biol Phys 74 567–74 [PubMed: 19046825]

Takahashi W, Yamashita H, Kida S, Masutani Y, Sakumi A, Ohtomo K, Nakagawa K and Haga A 2013 Verification of planning target volume settings in volumetric modulated arc therapy for stereotactic

body radiation therapy by using in-treatment 4-dimensional cone beam computed tomography Int J Radiat Oncol Biol Phys 86 426–31 [PubMed: 23562767]

Teoh M, Beveridge S, Wood K, Whitaker S, Adams E, Rickard D, Jordan T, Nisbet A and Clark CH 2013 Volumetric-modulated arc therapy (RapidArc) vs. conventional fixed-field intensity-modulated radiotherapy for (1)(8)F-FDG-PET-guided dose escalation in oropharyngeal cancer: a planning study Medical dosimetry : official journal of the American Association of Medical Dosimetrists 38 18–24 [PubMed: 22841937]

Verbakel WF, Cuijpers JP, Hoffmans D, Bieker M, Slotman BJ and Senan S 2009 Volumetric intensity-modulated arc therapy vs. conventional IMRT in head-and-neck cancer: a comparative planning and dosimetric study Int J Radiat Oncol Biol Phys 74 252–9 [PubMed: 19362244]

Wendling M, Zijp LJ, McDermott LN, Smit EJ, Sonke JJ, Mijnheer BJ and van Herk M 2007 A fast algorithm for gamma evaluation in 3D Med Phys 34 1647–54 [PubMed: 17555246]

Wijesooriya K, Aliotta E, Benedict S, Read P, Rich T and Larner J 2012 RapidArc patient specific mechanical delivery accuracy under extreme mechanical limits using linac log files Med Phys 39 1846–53 [PubMed: 22482606]

Wink N, Panknin C and Solberg TD 2006 Phase versus amplitude sorting of 4D-CT data J Appl Clin Med Phys 7 77–85 [PubMed: 16518319]

Woerner AJ, Choi M, Harkenrider MM, Roeske JC and Surucu M 2017 Evaluation of Deformable Image Registration-Based Contour Propagation From Planning CT to Cone-Beam CT Technol Cancer Res Treat 1533034617697242

Yin FF, Wang Z, Yoo S, Wu QJ, Kirkpatrick J, Larrier N, Meyer J, Willett CG and Marks LB 2008 Integration of cone-beam CT in stereotactic body radiation therapy Technol Cancer Res Treat 7 133–9 [PubMed: 18345702]

Zhao X and Zhang R 2020 Feasibility of 3D tracking and adaptation of VMAT based on VMAT-CT Radiother Oncol 149 18–24 [PubMed: 32416375]

Zhou L, Bai S, Zhang YB, Ming X, Zhang Y and Deng J 2018 Imaging Dose, Cancer Risk and Cost Analysis in Image-guided Radiotherapy of Cancers Scientific reports 8

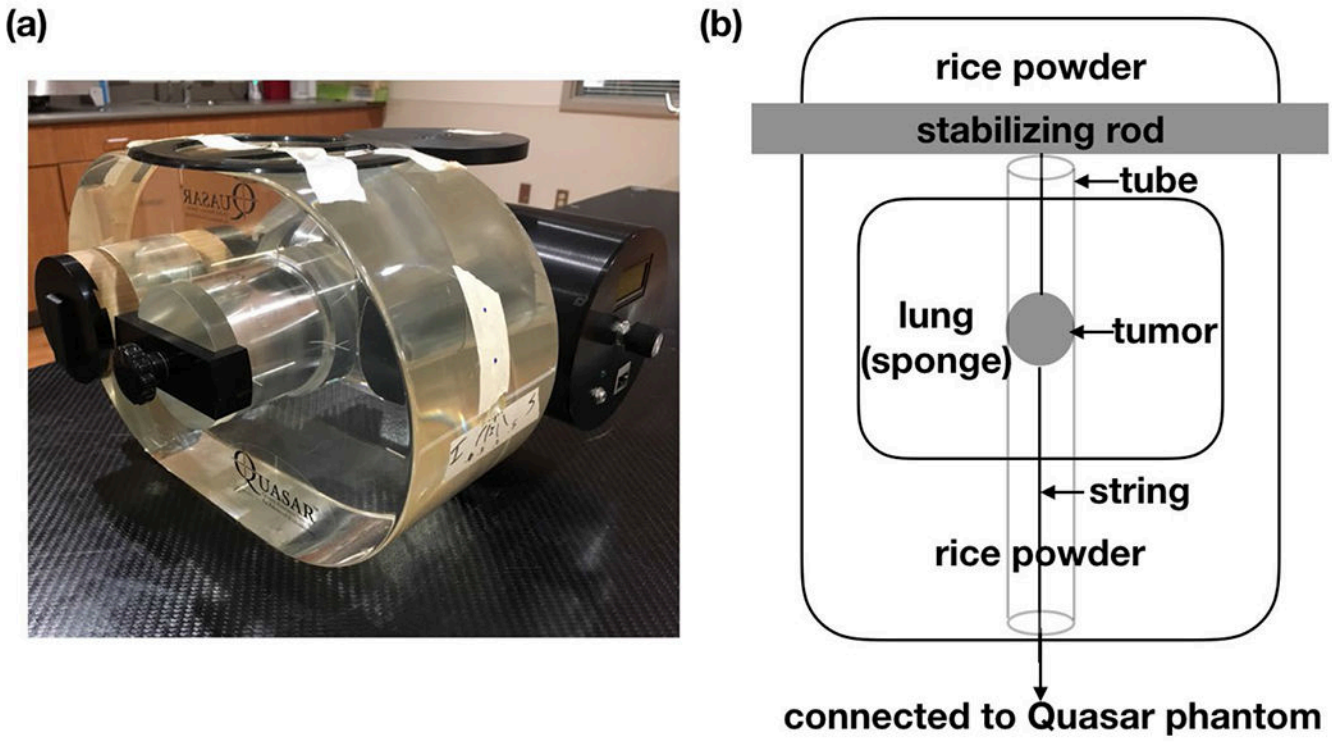

Figure 1.
(a) QUASAR phantom; (b) descriptive figure of an in-house deformable lung phantom.

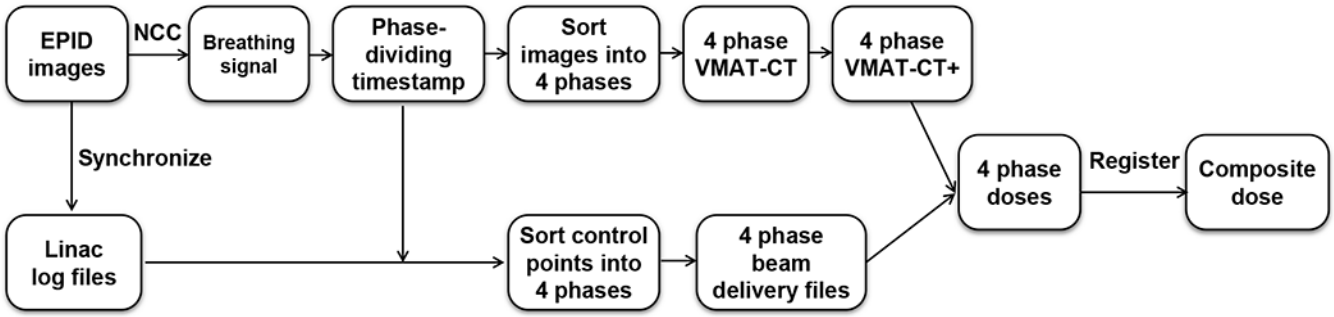

Figure 2.
Workflow of 4D dose reconstruction based on VMAT-CT+.

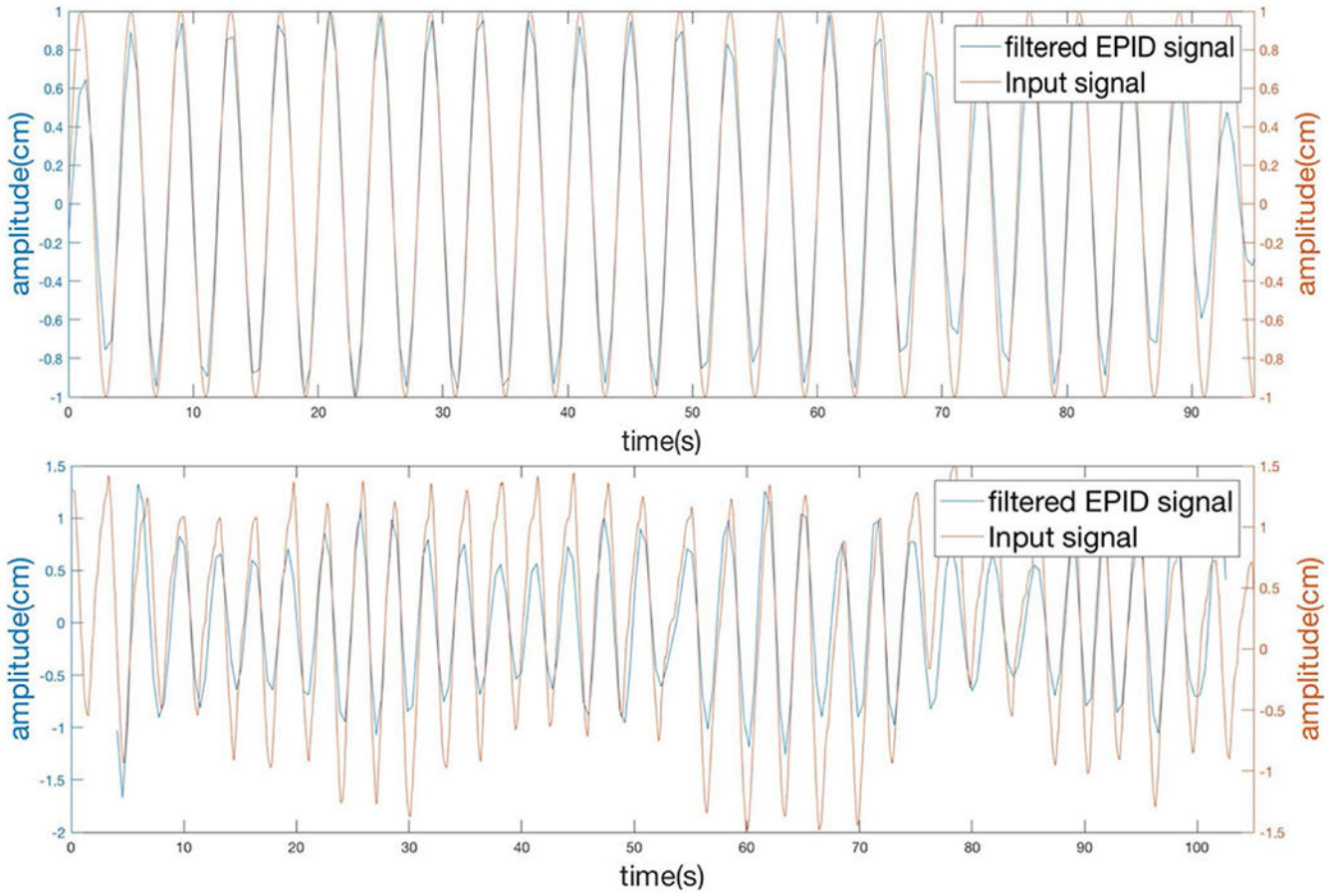

Figure 3.
Respiratory signals extracted from EPID images were synchronized with input signals to Quasar phantom. Top: regular sine wave breathing pattern. Bottom: irregular breathing pattern.

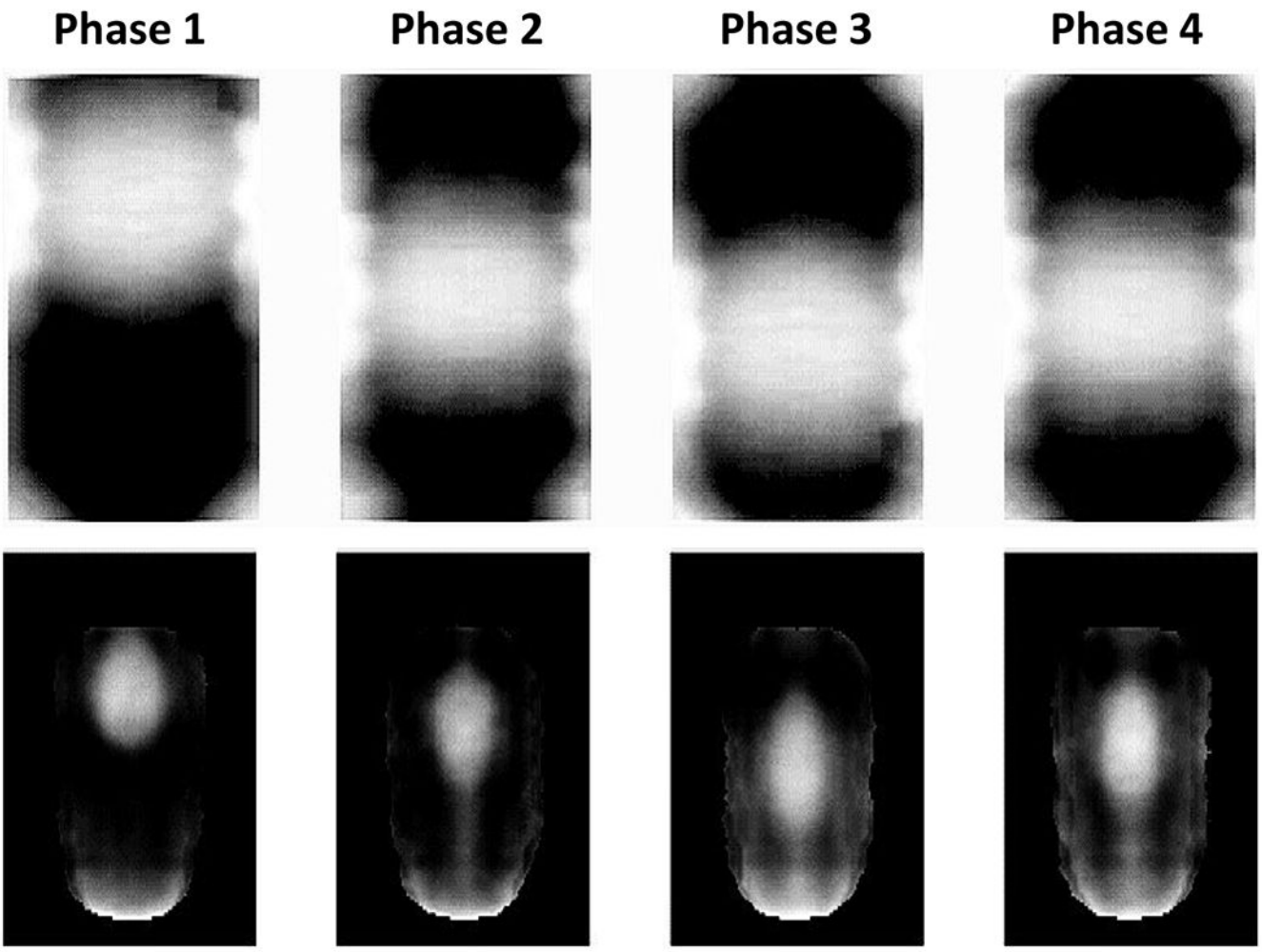

Figure 4.
Coronal view of reconstructed 4D VMAT-CT images of the QUASAR phantom (top) and the deformable phantom (bottom). Phases 1-4 refer to max exhale, mid-exhale-inhale, max inhale, and mid-inhale-exhale.

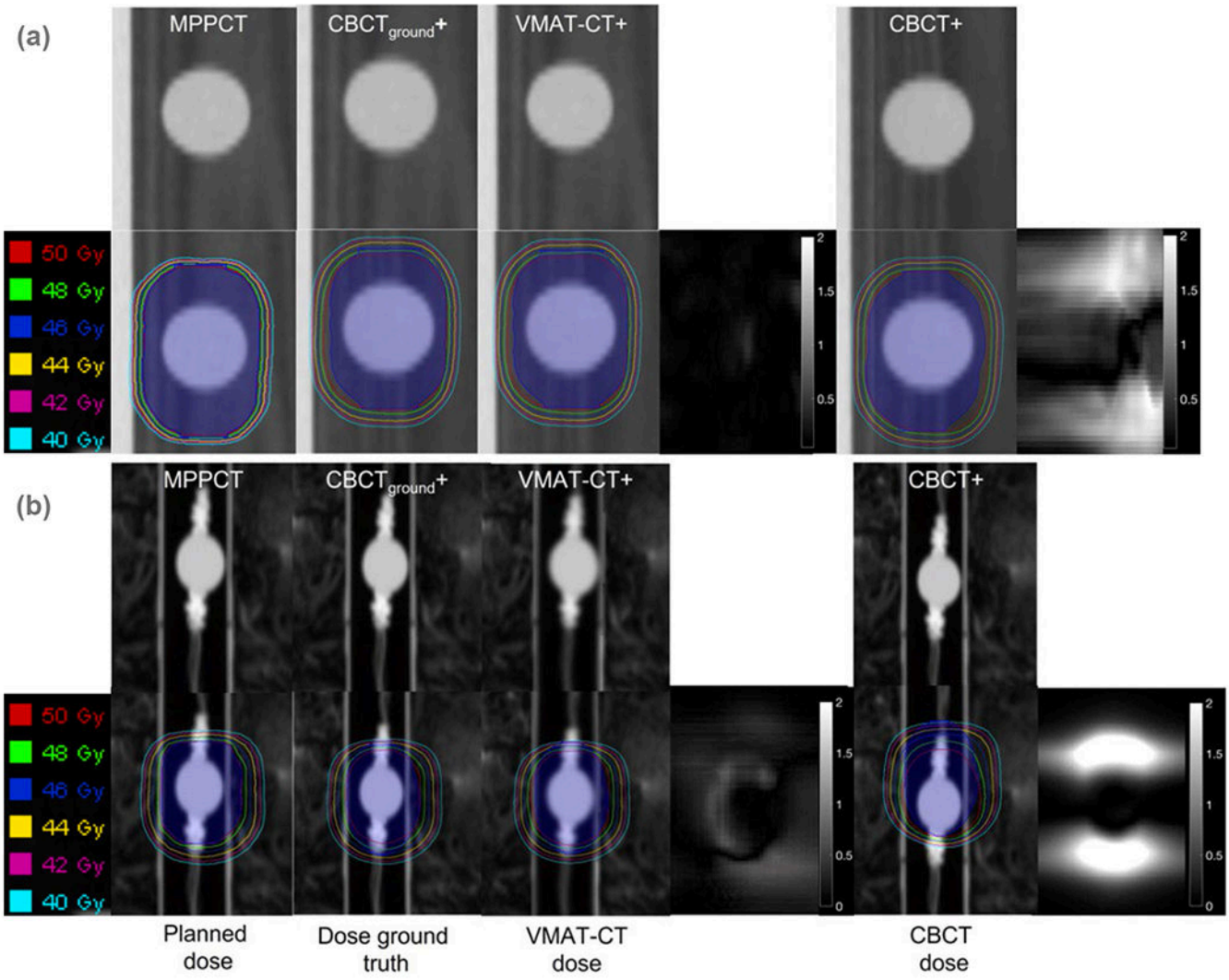

Figure 5.

4D tracking demonstrated on (a) a QUASAR phantom and (b) an in-house 4D deformable phantom. (From left to right) planned dose: dose distribution in the original plan; dose ground truth: dose based on CBCT$_{ground}$+; VMAT-CT dose: dose based on VMAT-CT+; 3D Gamma plot comparing VMAT-CT dose and dose ground truth; CBCT dose: dose based on pre-treatment CBCT+; 3D Gamma plot comparing CBCT dose and dose ground truth. The blue shaded area represents the original or new PTV.

Table 1.

Rigid registration uncertainties in 4D VMAT-CT.

Tries	X (mm)	Y (mm)	Z (mm)	Total (mm)
1	0.183	0.133	0.444	0.498
2	0.138	0.171	0.330	0.396
3	1.953	0.395	0.614	2.085
4	2.054	0.286	0.916	2.267
Mean	1.082	0.246	0.576	1.312
SD	1.065	0.119	1.255	1.002

SD: standard deviation.

Table 2.

Deformable registration uncertainties in 4D VMAT-CT.

Tries	HD (mm)	MDA (mm)	DSC	Jaccard coefficient
1	1.840	0.455	0.928	0.866
2	1.481	0.340	0.950	0.905
3	1.774	0.438	0.938	0.883
4	1.215	0.227	0.967	0.935
Mean	1.578	0.365	0.946	0.897
SD	0.288	0.105	0.017	0.030

SD: standard deviation; HD: Hausdorff distance; MDA: Mean distance to agreement; DSC: Dice similarity coefficient.